Journal of Materials Chemistry

Cite this: *J. Mater. Chem.*, 2012, **22**, 7961

www.rsc.org/materials

**PAPER**

# Controlled synthesis and luminescent properties of monodispersed PEI-modified $YVO_4:Bi^{3+},Eu^{3+}$ nanocrystals by a facile hydrothermal process†

**Yi-Chin Chen, Yun-Chen Wu, De-Yin Wang and Teng-Ming Chen***

***Received 8th February 2012, Accepted 22nd February 2012***
**DOI: 10.1039/c2jm30756a**

A series of water-soluble $YVO_4:Bi^{3+},Eu^{3+}$ nanocrystals, with surfaces functionalized by a branch polyethylenimine (BPEI) polymer, have been synthesized *via* a one-pot hydrothermal method. It was found that the particle size and crystal morphology could be efficiently controlled by different reaction temperatures, pH values and molecular weights of the BPEI polymer. The surface modification of the nanocrystals was characterized using Fourier transform infrared spectroscopy (FT-IR). The highly crystalline $YVO_4:Bi^{3+},Eu^{3+}$ nanoparticles, with an average diameter of 20 nm, can be dispersed in water due to the presence of amino ligands. When conjugated with biomolecules, the $YVO_4:Bi^{3+},Eu^{3+}$ nanocrystals retain their strong red emission, peaking at 619 nm under near-ultraviolet (n-UV) excitation. The results indicate that $YVO_4:Bi^{3+},Eu^{3+}$ nanocrystals can serve as a promising candidate for biological imaging, and immunoassay applications.



## 1. Introduction

Over the past few decades, increasing efforts have been made to explore the use of fluorescent materials for biological applications.[1–5] Currently, the most common approach is the application of fluorescent organic molecules and quantum dots (QDs). However, it is generally felt that organic dyes and QDs exhibit problematic weak photostability, a broad emission band, short luminescence lifetimes, photoblinking, and toxicity problems.[6,7] These drawbacks limit fluorescent labeling in clinical diagnosis, DNA sequencing and immunoassays. Recently, several fluorescence probes using lanthanide (Ln)-doped fluoride and oxide nanocrystals have been demonstrated to be effective for biological detection.[8–11] The fluoride nanocrystal has the advantages of a low phonon energy and a high up-conversion efficiency when pumped with infrared excitation.[12,13] Nevertheless, it is also characterized as having low chemical stability and low water dispersibility. Accordingly, it is important to start developing oxide nanocrystals for biological applications because of their chemical stability and nontoxic properties.

Yttrium orthovanadate doped with $Ln^{3+}$ ($YVO_4:Ln^{3+}$) is a well-known, highly efficient optical material with a variety of emitting colors, which has been extensively used for lighting, displays and laser technology.[14–16] Of the many $Ln^{3+}$ ions, the $Eu^{3+}$ ion usually shows strong red line emissions due to the parity forbidden characteristics of the 4f–5d transitions.[17–19] The first scientific report on $Eu^{3+}$-doped $YVO_4$ as a new red phosphor for cathode ray tubes (CRT) was in 1964.[20] The combination of a relatively red emission (~615 nm) under UV excitation, good color purity and high luminescence efficiency (>70%) made this material ideally appropriate for fluorescent applications.[21] Recently, a variety of synthesis methods of $YVO_4:Eu^{3+}$ crystalline nanoparticles have been reported, including co-precipitation,[15,22] microwave assistance, sol–gel thermolysis,[23,24] micro-emulsion,[25] a hydrothermal/solvothermal process,[26–29] *etc.* Modified syntheses *via* the hydrothermal/solvothermal method have also been developed in order to improve the size and dispersion of the $YVO_4$ nanocrystals.[15,17,22–29] However, it is still a challenge to use the surface-functionalized and monodispersed nanocrystals for bio-imaging and drug delivery applications.

In this work, we present a facile one-step hydrothermal route for water-soluble and amino group functionalized $YVO_4:Bi^{3+},Eu^{3+}$ nanocrystals, with controllable particle size and crystal morphology. We also proposed a crystal growth mechanism related to the protonation behavior of the cationic surfactant branch-polyethylenimine (BPEI) polymer in different pH value environments. The relevant properties of $YVO_4:Bi^{3+},Eu^{3+}$ nanocrystals were investigated using X-ray diffraction (XRD), X-ray photoelectron spectrometry (XPS), scanning electron microscopy (SEM), transmission electron microscopy (TEM), dynamic light scattering (DLS), Fourier transform infrared spectroscopy (FT-IR) and photoluminescence (PL) spectrometry.

*Phosphors Research Laboratory, Department of Applied Chemistry and Institute of Molecular Science, National Chiao Tung University, Hsinchu 30010, Taiwan. E-mail: tmchen@mail.nctu.edu.tw; Tel: +886-3-5731695*

† Electronic supplementary information (ESI) available: EDX spectrum of $YVO_4:Bi^{3+},Eu^{3+}$ nanocrystals synthesized with high molecular weight BPEI polymer under different pH conditions. See DOI: 10.1039/c2jm30756a

## 2. Experimental

### 2.1 Materials and reagents

$Y(NO_3)_3 \cdot 6H_2O$ (Aldrich), $Eu(NO_3)_3 \cdot 5H_2O$ (Aldrich), $Bi(NO_3)_3 \cdot 5H_2O$ (Merck), $NH_4VO_3$ (Showa), branched-polyethylenimine (BPEI) solution (Aldrich, $M_w = 2000$ and $M_w = 20\,000$), bovine serum albumin (BSA) (Aldrich), 2-(*N*-morpholino)ethanesulfonic acid (MES) solution (Aldrich), sulfo-*N*-hydroxysuccinimide (Sulfo-NHS) (Thermo), and 1-ethyl-3-(3-dimethylaminopropyl)carbodiimide (EDC) (Thermo) were of analytical grade and were used as received without further purification.

### 2.2 Synthesis of $YVO_4$:$Bi^{3+}$,$Eu^{3+}$ nanocrystals

In a typical synthesis, 1 mmol $Y(NO_3)_3 \cdot 6H_2O$ and the required amount of $Ln(NO_3)_3 \cdot 5H_2O$ (Ln = Bi and Eu) were dissolved in 10 ml deionized water (DIW) and stirred at room temperature to afford a transparent solution. In another vessel, 1 mmol $NH_4VO_3$ was dissolved in 10 ml solution of sodium hydroxide at pH = 12, and the aqueous solution was added dropwise to the $Ln(NO_3)_3$ solution and stirred at room temperature for 0.5 h (Y : Bi : Eu : V = 0.7 : 0.15 : 0.15 : 1). Next, 0.04 g $ml^{-1}$ BPEI solution was added to the mixed solution and 1 M NaOH aqueous solution was added dropwise to tune the final pH of the growth solution to 4, 7, and 11. After stirring for 1 h at 80 °C, the obtained mixture was transferred into a 100 ml Teflon-lined autoclave for a 24 h hydrothermal treatment at 180 °C and it was then cooled to room temperature naturally. The resulting products were collected by centrifugation, washed with distilled water several times, and dried at 80 °C for 24 h in an oven.

### 2.3 Conjugation of $YVO_4$:$Bi^{3+}$,$Eu^{3+}$ nanocrystals with biomolecules

BSA (10 mg) was dissolved in 100 mM MES buffer (pH = 5.9), and the amino group modified $YVO_4$:$Bi^{3+}$,$Eu^{3+}$ nanocrystals (0.1, 0.5, 1.0 mg) were resuspended in MES buffer. Sulfo-NHS (50 mM) and EDC (50 mM) solution were mixed with BSA solution. The mixture was incubated for 0.5 h at room temperature with vigorous shaking. After incubation, $YVO_4$:$Bi^{3+}$,$Eu^{3+}$ nanocrystals were added to the mixture, and reacted for 24 h at 4 °C overnight. All impurities were removed by centrifugation and the products were washed with phosphate buffered saline (PBS). The samples were electrophoresed on a 10% sodium dodecyl sulfate polyacrylamide gel electrophoresis (SDS-PAGE). The electrophoresis was performed with a 1X SDS-PAGE running buffer at 90 V for 30 min followed by 120 V for 1.5 h. The SDS-PAGE was stained with a stain buffer containing Coomassie Brilliant blue R-250 for 0.5 h and destained with destain buffer I (methanol–acetic acid–water = 4 : 1 : 5, v/v/v) for 20 min and followed by destain buffer II (methanol–acetic acid–water = 1.2 : 0.05 : 8.75) overnight. The protein concentrations of the samples were measured using a bicinchoninic acid (BCA) protein assay kit (Aldrich).

### 2.4 Characterization

The phase purity of the obtained products was analyzed by powder X-ray diffraction (XRD) using a Bruker AXS D8 advanced automatic diffractometer with Cu-K$\alpha$ radiation ($\lambda$ = 1.5405 Å, 40 kV × 20 mA). The surface components and composition of the samples were measured on a high resolution X-ray photoelectron spectrometer (PHI Quantera SXM; ULVAC-PHI). The particle sizes of the products were analyzed by a Brookhaven 90 plus dynamic light scattering (DLS) particle size analyzer equipped with a 35 mW He–Ne laser. All DLS measurements were carried out with a wavelength of 632.8 nm at 25 °C with a 90° angle of detection. The morphology and composition of the samples were inspected using a field emission scanning electron microscope (FE-SEM; JSM-7401F, JEOL) and a field emission gun transmission electron microscope (FEG-TEM; JEM-2100F, JEOL) with a Link ISIS 300 energy dispersive X-ray analyzer (EDX). The selected area electron diffraction (SAED) patterns were obtained using FEG-TEM operating at 200 kV. Fourier transform infrared spectroscopy (FT-IR) spectra were recorded on a Nicolet Avatar 320 infrared spectrometer using the KBr pellet technique. The photoluminescence (PL)/photoluminescence excitation (PLE) spectra and transient decays were recorded on a Spex FluoroLog-3 spectrofluorometer equipped with a 450 W Xe lamp and cutoff filters to avoid the second-order emissions of the source radiation.

## 3. Results and discussion

### 3.1 Crystal structure and morphology

Fig. 1 shows the collected XRD data of the as-synthesized $YVO_4$:$Bi^{3+}$,$Eu^{3+}$ nanocrystals with BPEI polymer of different molecular weights, synthesized at pH = 4, 7 and 11, respectively. To ensure the phase purity, the diffraction peaks of the $YVO_4$:$Bi^{3+}$,$Eu^{3+}$ nanocrystals are indexed on the basis of single crystal $YVO_4$ data (ICSD No. 78074), with a tetragonal structure. The results show a single phase with no unidentified diffraction peaks from impurities. In the crystal structure of $YVO_4$, there is only one crystallographically distinct site for the Y atoms. For the $YVO_4$:$Bi^{3+}$,$Eu^{3+}$ nanocrystals, as both the $Eu^{3+}$ and $Y^{3+}$ ions have the same valence and atomic radius, there are no charge compensation issues for isovalent substitution. The calculated lattice parameters of $a = b = 7.15$ Å and $c = 6.31$ Å are also consistent with the standard lattice contents $a = b = 7.12$ Å and $c = 6.29$ Å.[30] As a whole, the sharp diffraction peaks of the different nanocrystalline $YVO_4$:$Bi^{3+}$,$Eu^{3+}$ samples suggest that high crystallinity can be obtained using the BPEI polymer with different molecular weights at a relatively low reaction temperature (180 °C) during hydrothermal treatment.

XPS has been proven to be a successful technique for qualitatively determining the surface components and composition of the sample. Fig. 2a shows the photoelectron survey spectrum of the $YVO_4$:$Bi^{3+}$,$Eu^{3+}$ nanocrystals with the binding energy ranging from 0 to 1100 eV. It can be seen that the $YVO_4$:$Bi^{3+}$,$Eu^{3+}$ nanocrystal contains Y, V and O elements, with no other extant elements except for carbon. The carbon results from the hydrothermal process, in which some additives were employed. Fig. 2b and 2c show the respective element data for the XPS measurements. Two splitting lines: Y $3d_{5/2}$ (1160.6 eV), and Y $3d_{3/2}$ (162.6 eV), were observed in the binding energy of the Y 3d states. Otherwise, the V 2p states were split into V $2p_{3/2}$ (519.9 eV) and V $2p_{1/2}$ (527.4 eV) with an energy splitting

 

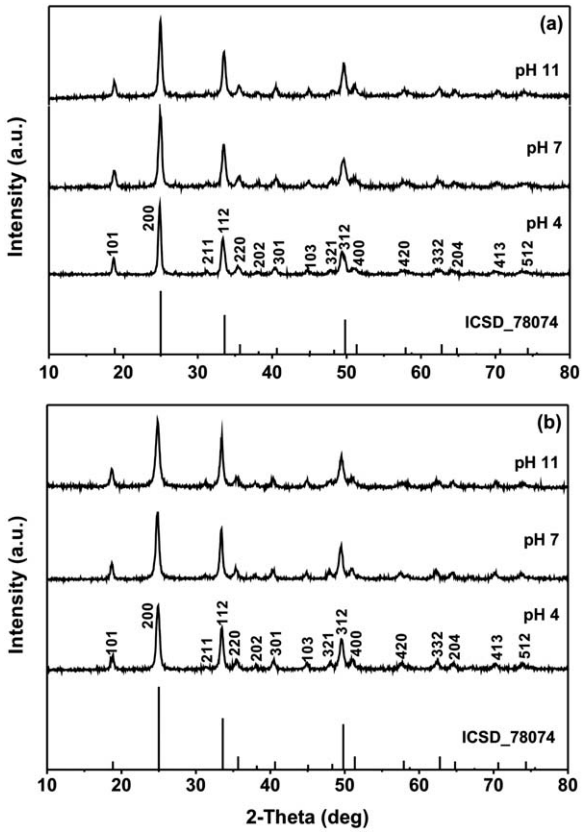


**Fig. 1** XRD patterns of $YVO_4$:$Bi^{3+}$,$Eu^{3+}$ nanocrystals prepared by a hydrothermal method using (a) low molecular weight BPEI polymer, (b) high molecular weight BPEI polymer at pH = 4, 7, and 11. The standard data for tetragonal $YVO_4$ (ICSD No. 78074) was used as reference.

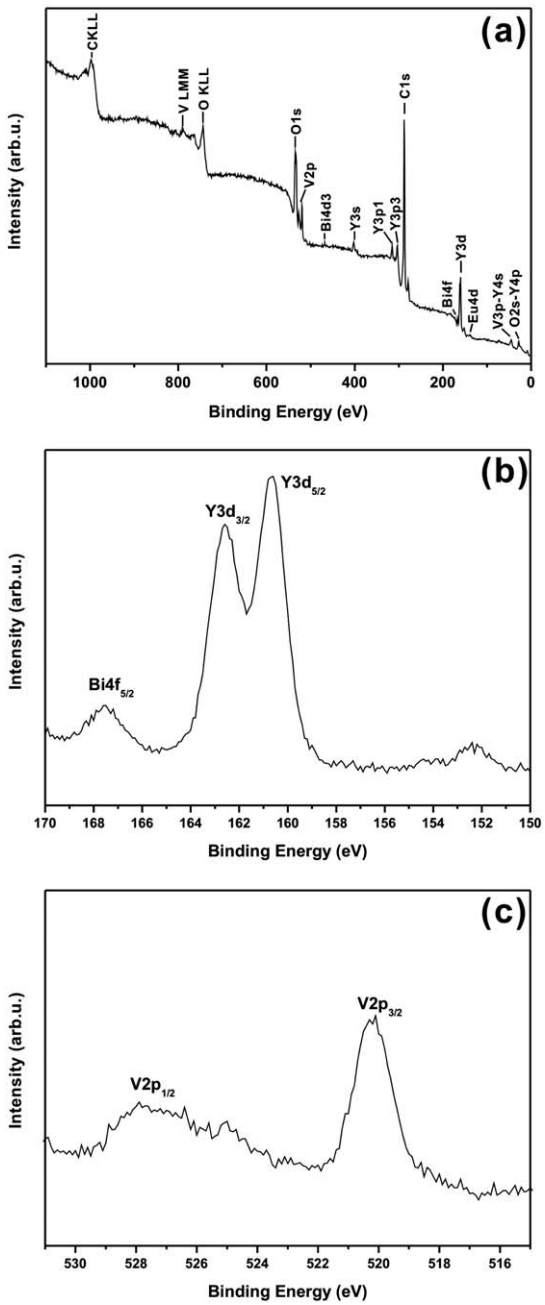


**Fig. 2** XPS spectra of $YVO_4$:$Bi^{3+}$,$Eu^{3+}$ nanocrystal in the range of (a) 0–1100 eV, (b) 150–170 eV, and (c) 515–535 eV.

of $\Delta$ = 7.5 eV, due to the spin–orbit interactions. The doped elements: Bi 4f (166.8 eV) and Eu 4d (136.6 eV), were also detected in the $YVO_4$:$Bi^{3+}$,$Eu^{3+}$ nanocrystals.

Fig. 3 shows the SEM characterization of the particle size and morphology for the as-synthesized $YVO_4$:$Bi^{3+}$,$Eu^{3+}$ nanocrystals using the BPEI polymer with a low molecular weight ($M_w$ = 2000). To obtain insight into the influence of the polymer, we also investigated the particle using TEM. The sample (pH = 4) synthesized with the low molecular weight polymer was composed of many irregularly shaped sheets. With the pH value increasing to 7, the sample starts to form regular granular-like particles with an average diameter of ~20 nm, and weak aggregation. When the pH value increases to 11, it could be seen from the SEM images that the obtained particles show an irregular rod-like shape. The TEM images show similar results compared to the SEM images; it is evident that most of the particles are affected by different pH conditions. This will be discussed later.

As shown in Fig. 3b, 3d and 3f, the samples synthesized at pH = 4 and 7 consist of single crystalline nanoparticles, whereas the sample synthesized at pH = 11 is made up of several granular-like crystalline nanoparticles. The $YVO_4$:$Bi^{3+}$,$Eu^{3+}$ nanocrystals using the BPEI polymer with a high molecular weight ($M_w$ = 20 000) at different pH values are also investigated in Fig. 4. The as-prepared sample (pH = 4) is mainly composed of square nanoplates ~50 nm thick. The SEM results for the $YVO_4$:$Bi^{3+}$,$Eu^{3+}$ nanocrystal in acidic conditions show a typical tetragonal-like morphology of the $YVO_4$ crystal, which can be ascribed to the tetragonal $I4_1/amd$ crystal structure. With a further increase of the pH value to 7, the sample shows a granular-like morphology, which is similar to the sample using the low molecule weight BPEI polymer. The particle size estimated from the number average was also ~20 nm. When the pH value is increased to 11, the primary nanoparticles tend to agglomerate and form olive-like polycrystalline nanorods that are, on average, ~100 nm in length. In a sense, this suggests that the particle size and morphology of the samples (pH = 7 and 11) are not influenced by the molecular weight of the polymer;

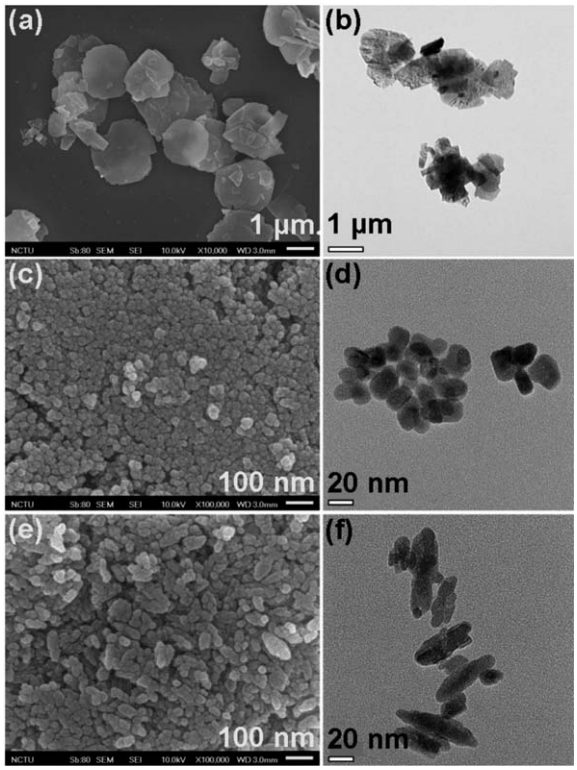


**Fig. 3** SEM and TEM images of $YVO_4$:$Bi^{3+}$,$Eu^{3+}$ nanocrystals synthesized at 180 °C for 24 h and with pH values of (a,b) pH 4, (c,d) pH 7, and (e,f) pH 11. All samples were prepared with the low molecular weight BPEI polymer by hydrothermal treatment.

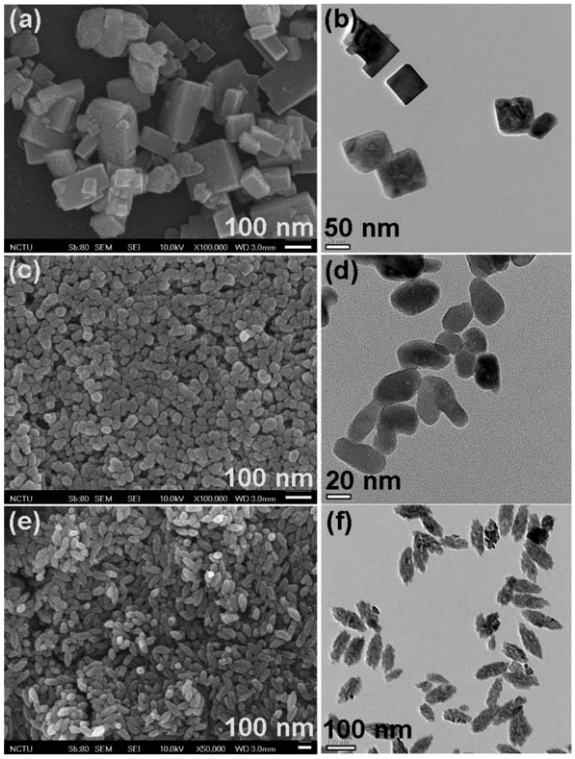


**Fig. 4** SEM and TEM images of $YVO_4$:$Bi^{3+}$,$Eu^{3+}$ nanocrystals synthesized at 180 °C for 24 h and with a pH value of (a,b) pH 4, (c,d) pH 7, and (e,f) pH 11. All samples were prepared with the high molecular weight BPEI polymer by hydrothermal treatment.

however, the use of a high molecular weight polymer does lead to better uniformity and dispersion.

The TEM images also confirm the above results, as can be seen in Fig. 4b, 4d and 4f. According to the SEM and TEM results, the following discussion will focus on the samples synthesized using the BPEI polymer with a high molecular weight. The size and polydispersity of the as-prepared samples were characterized by DLS measurement. Fig. 5a demonstrates an illustration of the quantity of two dispersions for the tetragonal particle, *i.e.*, ~54.1 nm for height, ~338.2 nm for length and width, consistent with the observed size from the TEM image. Fig. 5b and 5c each show only one population: one has a peak diameter of ~20.3 nm, and the other has a peak diameter of ~98.2 nm. These results are also consistent with the observed sizes from the TEM images.

As shown in Fig. 6, the HRTEM images and the SAED patterns of the individual nanocrystal were used to study the crystallinity from its diffraction pattern. The HRTEM images show a perfect crystallite surface, in which the distances between adjacent lattice fringes are estimated for each sample. The calculated 0.35 and 0.46 nm lattice spacings, corresponding to the (200) and (101) interplanar distance of the samples synthesized at pH = 4 and 11, infer the preferential growth direction. Also, the sample synthesized at pH = 7 clearly demonstrates that the lattice fringes corresponding to the (220) and (200) planes were separated by 0.25 and 0.35 nm. The results can be indexed to diffractions from the (101), (200) and (220) planes of the tetragonal structure, in accordance with the XRD patterns. The sharp spots in the SAED patterns of the samples synthesized at

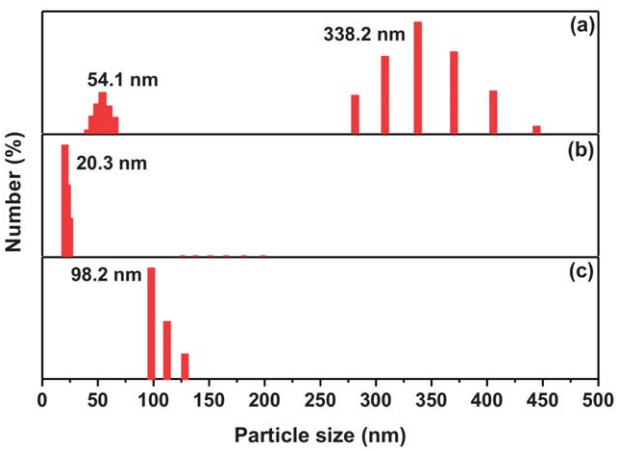


**Fig. 5** DLS analysis of $YVO_4$:$Bi^{3+}$,$Eu^{3+}$ nanocrystals synthesized with the high molecular weight BPEI polymer under different pH conditions. (a) pH 4, (b) pH 7, and (c) pH 11.

pH = 4 and 7 exhibit highly ordered lattice ordering, which suggests the single crystalline nature of the $YVO_4$:$Bi^{3+}$,$Eu^{3+}$ crystalline nanoparticles. Furthermore, the annular spots of the SAED patterns of the sample synthesized at pH = 11 clearly verify the polycrystalline nature of the $YVO_4$:$Bi^{3+}$,$Eu^{3+}$ crystalline nanoparticles. The compositions of the obtained samples are confirmed by EDX analysis. Fig. S1† shows the EDX patterns of the $YVO_4$:$Bi^{3+}$, $Eu^{3+}$ nanocrystals, which reveal the homogeneous distribution of Y/V/O/Bi/Eu in the solid. The details of the

 

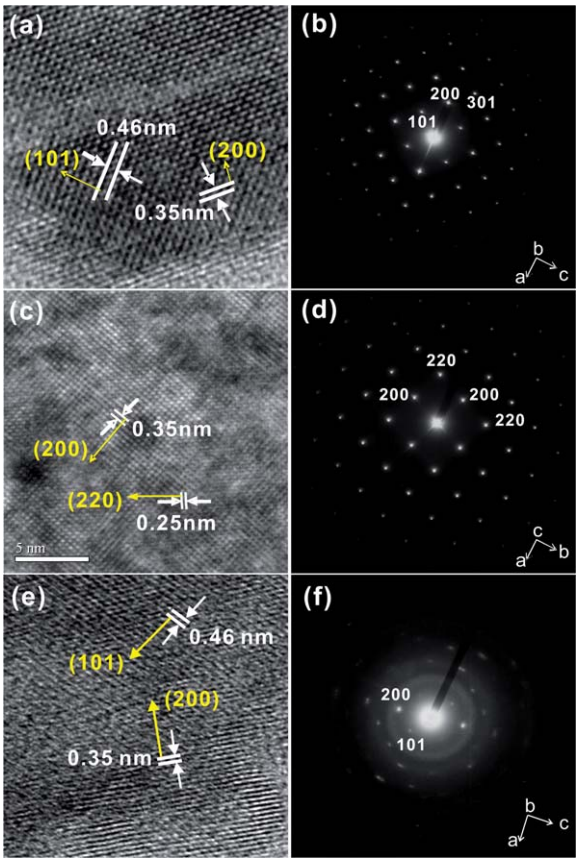


**Fig. 6** HRTEM images and SAED patterns of $YVO_4$:$Bi^{3+}$,$Eu^{3+}$ nanocrystals synthesized with high molecular weight BPEI under different conditions. (a,b) pH 4, (c,d) pH 7, and (e,f) pH 11.

EDX spectra are summarized in Table S1.† It should be noted that the Bi atomic percentage of the sample (pH = 4) is much lower than those of the others.

To characterize the surface properties, the FT-IR absorption spectra of the $YVO_4$:$Bi^{3+}$,$Eu^{3+}$ nanocrystals were measured. The bulk $YVO_4$:$Bi^{3+}$,$Eu^{3+}$ sample synthesized by solid-state reaction was also presented as a comparison. As shown in Fig. 7, a strong absorption band at ~810 $cm^{-1}$ and a weak band at ~451 $cm^{-1}$ are attributed to the V–O (from the $VO_4^{3-}$ group) and the Y–O stretching vibrations of the host lattice, respectively. The broad band at ~3407 $cm^{-1}$ corresponds to the O–H or N–H stretching vibrations, while the bands at 1633 and 1385 $cm^{-1}$ are related to the bending vibrations of the N–H bond in the BPEI polymer. The weak bands at 2923 and 2849 $cm^{-1}$ can be assigned to the asymmetric and symmetric stretching vibrations of the $–CH_2$ in the BPEI polymer. The details of the peak assignments for the samples prepared at pH = 4, 7 and 11 are presented in Table 1. These results indicate that the as-prepared $YVO_4$:$Bi^{3+}$,$Eu^{3+}$ nanocrystals contain amino groups on the surfaces, which play an important role in conjugation with biomolecules for bio-applications.

### 3.2 Mechanism of crystal growth

In this work, the BPEI polymer acts as a chelating and protective agent that can further influence the size and morphology of the final products because the nitrogen atoms in the main and side chains of the polymer can serve as electron donors for chelating the metal ions. Therefore, due to the stronger chelating ability of the high molecular weight BPEI polymer, it is able to bind tightly to the surface of the nanoparticles, and hence control the

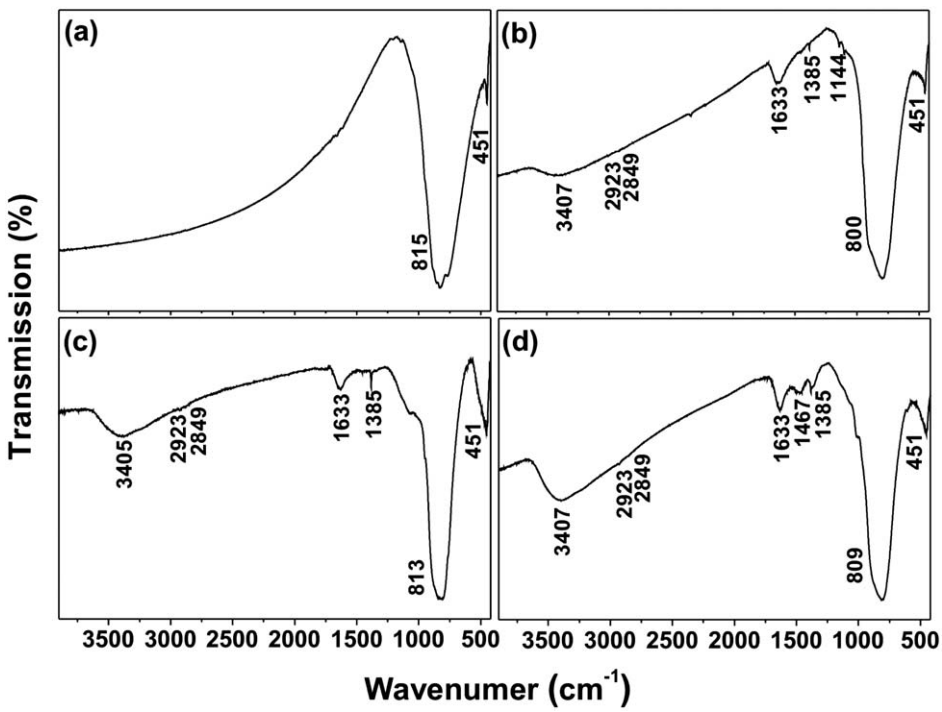


**Fig. 7** Comparison of the FT-IR spectra for (a) bulk $YVO_4$:$Bi^{3+}$,$Eu^{3+}$ prepared by the solid-state method; $YVO_4$:$Bi^{3+}$,$Eu^{3+}$ nanocrystals synthesized with high molecular weight BPEI polymer under different pH conditions: (b) pH 4, (c) pH 7, and (d) pH 11.

**Table 1** The detailed FT-IR spectral peak assignments for $(Y_{0.7}Bi_{0.15}Eu_{0.15})VO_4$ NPs under different pH conditions

| | Band position/cm$^{-1}$ | | | |
|---|---|---|---|---|
| Assignment | Annealed | pH 4 | pH 7 | pH 11 |
| N–H stretching vibration | — | 3407 | 3405 | 3407 |
| $CH_2$ asymmetric stretching | — | 2923 | 2923 | 2923 |
| $CH_2$ symmetric stretching | — | 2849 | 2849 | 2849 |
| $CH_2$ deformation vibration | — | — | — | 1467 |
| N–H bending vibration | — | 1633/1385 | 1633/1385 | 1633/1385 |
| C–N stretching vibration | — | 1144 | — | — |
| V–O stretching vibration | 815 | 800 | 813 | 809 |
| Y–O stretching vibration | 451 | 451 | 451 | 451 |

growth of the $YVO_4$:$Bi^{3+}$,$Eu^{3+}$ nanocrystals, and disperse the nanoparticles.

In addition, the effects of the pH values on the size and morphology were investigated. First, it is noted that the protonation behaviors of the BPEI polymer at different pH values have been reported.[31–33] When the pH value decreases to a low range, the degree of protonation increases, and the polymer tends to form a loose structure with a rich positive charge. The deprotonated amines form a complex with the lanthanide metal ions, which are revealed on the crystal surface *via* coordination, and each protonated amino group is highly restricted for coordination to a metal ion because of strong neighboring electrostatic repulsion. Therefore, the BPEI polymer acts as a capping agent to adsorb on the specific crystal facet, and restricts the crystal growth in order to form sheet- or square-like morphologies, in this case. On the other hand, at a high pH range, the BPEI polymer tends to shrink from the reduced solvation power of the protonated polymer. Most of the deprotonated amines coordinate to metal ions, and the strong neighboring interactions of the polymer molecules cause the aggregation of crystal seeds, and form polycrystalline nanoparticles.

### 3.3 Spectroscopic characterization of the $YVO_4$:$Bi^{3+}$,$Eu^{3+}$ nanocrystals

Fig. 8 shows the PLE/PL spectra of the $YVO_4$:$Bi^{3+}$,$Eu^{3+}$ nanocrystals synthesized at pH = 4, 7 and 11. As can be seen from the PLE spectra (monitored at 619 nm), the absorption band peaking at ~285 nm for the $YVO_4$:$Bi^{3+}$,$Eu^{3+}$ nanocrystals synthesized at pH = 4, 7 and 11 is attributed to the charge transfer from the oxygen ligands to the central vanadium atom within the $VO_4^{3-}$ group. The UV energy absorbed by the $VO_4^{3-}$ groups is subsequently transferred to $Eu^{3+}$ by a nonradiative transfer process in all of the samples. Noticeably, the band edges of the excitation band of the samples prepared at pH = 7 and 11 extend from 375 nm to 425 nm and the maximum of the excitation band shifts to 345 nm. These observations suggest that the extension of the excitation band originated from the metal–metal charge transfer transitions from the $Bi^{3+}$ to the $V^{5+}$ ion rather than the $6s^2$–6s6p transition of $Bi^{3+}$; then, the energy is transferred to the $Eu^{3+}$ ion.[34] The sharp excitation band at 395 nm corresponds to the $^7F_0$–$^5L_6$ transition within the $4f^6$ configuration of the $Eu^{3+}$ ions.

The PL spectra of the $YVO_4$:$Bi^{3+}$,$Eu^{3+}$ nanocrystals synthesized at pH = 4, 7 and 11 show a typical linear feature for the $Eu^{3+}$ emission, peaking at 619 nm, and ranging from 580 nm to 730 nm, which can be ascribed to the radiative transitions from the $^5D_0$ to the $^7F_J$ ($J$ = 1, 2, 3, 4) levels of the $Eu^{3+}$ ion. By comparing the maximum emission intensity at 619 nm, the obtained $YVO_4$:$Bi^{3+}$, $Eu^{3+}$ nanocrystals prepared at pH = 4 show a much lower emission intensity than those prepared at pH = 7 and 11. In the present synthesis, the $Bi(NO_3)_3$ reacted with water and formed the intermediate product $BiONO_3$, which further reacted with $VO_3^-$ and generated $Bi^{3+}$-doped $YVO_4$ precursors. When the reaction is in acidic conditions, the formation of the intermediate product is regarded as restricted because of the inert

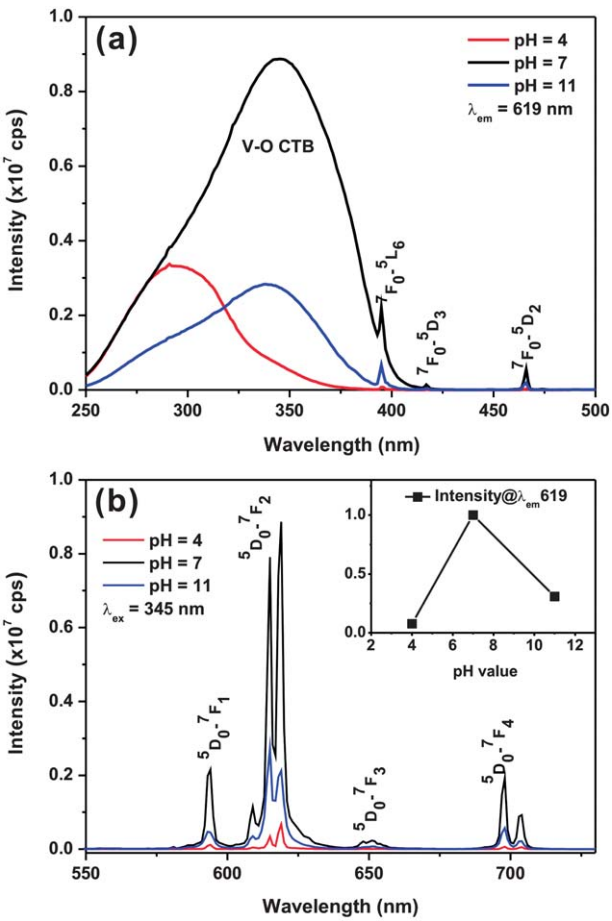


**Fig. 8** (a) PLE spectra of $YVO_4$:$Bi^{3+}$,$Eu^{3+}$ nanocrystals. (b) PL spectra of $YVO_4$:$Bi^{3+}$,$Eu^{3+}$ nanocrystals. The inset shows the relative integrated PL intensity ($\lambda_{ex}$ = 345 nm) of the $YVO_4$:$Bi^{3+}$, $Eu^{3+}$ nanocrystals.

 

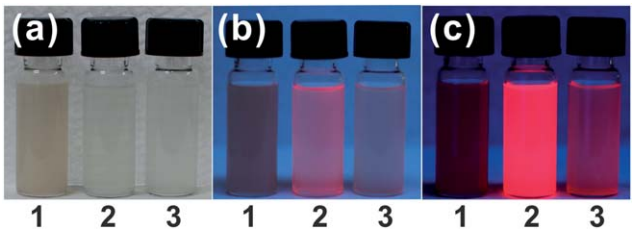


**Fig. 9** The photos show the luminescence of different $YVO_4:Bi^{3+},Eu^{3+}$ nanocrystals under (a) daylight, (b) 254 nm, and (c) 365 nm excitations. Samples are prepared by hydrothermal methods at pH = 4 (sample 1), pH = 7 (sample 2), and pH = 11 (sample 3), respectively. All samples are suspended in DIW.

reactivity of the $Bi^{3+}$ ions. When the pH value rises to 11, the polycrystalline nanoparticles show relatively weak emission in comparison to the $YVO_4:Bi^{3+},Eu^{3+}$ nanocrystals synthesized at pH = 7, presumably because of the large surface area of the polycrystalline nanorods which introduces more defects into the $YVO_4:Bi^{3+},Eu^{3+}$ nanocrystals. These defects provide non-radiative recombination pathways as fluorescence quenching centers, and thus cause a decrease in the photoluminescence intensity. Fig. 9 shows the luminescence of the $YVO_4:Bi^{3+}$, $Eu^{3+}$ nanocrystals under ambient light, 254 and 365 nm excitations. The sample prepared at pH = 7 exhibits a strong red emission under UV excitation.

The representative decay curves for the luminescence of the $YVO_4:Bi^{3+},Eu^{3+}$ nanocrystals are shown in Fig. 10. The decay kinetics behavior depends on the number of different luminescent centers, defects, energy transfer and impurities in the host. In the case of the $YVO_4:Bi^{3+},Eu^{3+}$ nanocrystals, the $Eu^{3+}$ ions occupy the sites of the $Y^{3+}$ ions with $D_{2d}$ symmetry, implying only one luminescence center. The room temperature decay dynamic monitors the $^5D_0$–$^7F_2$ transitions at 619 nm for $Eu^{3+}$

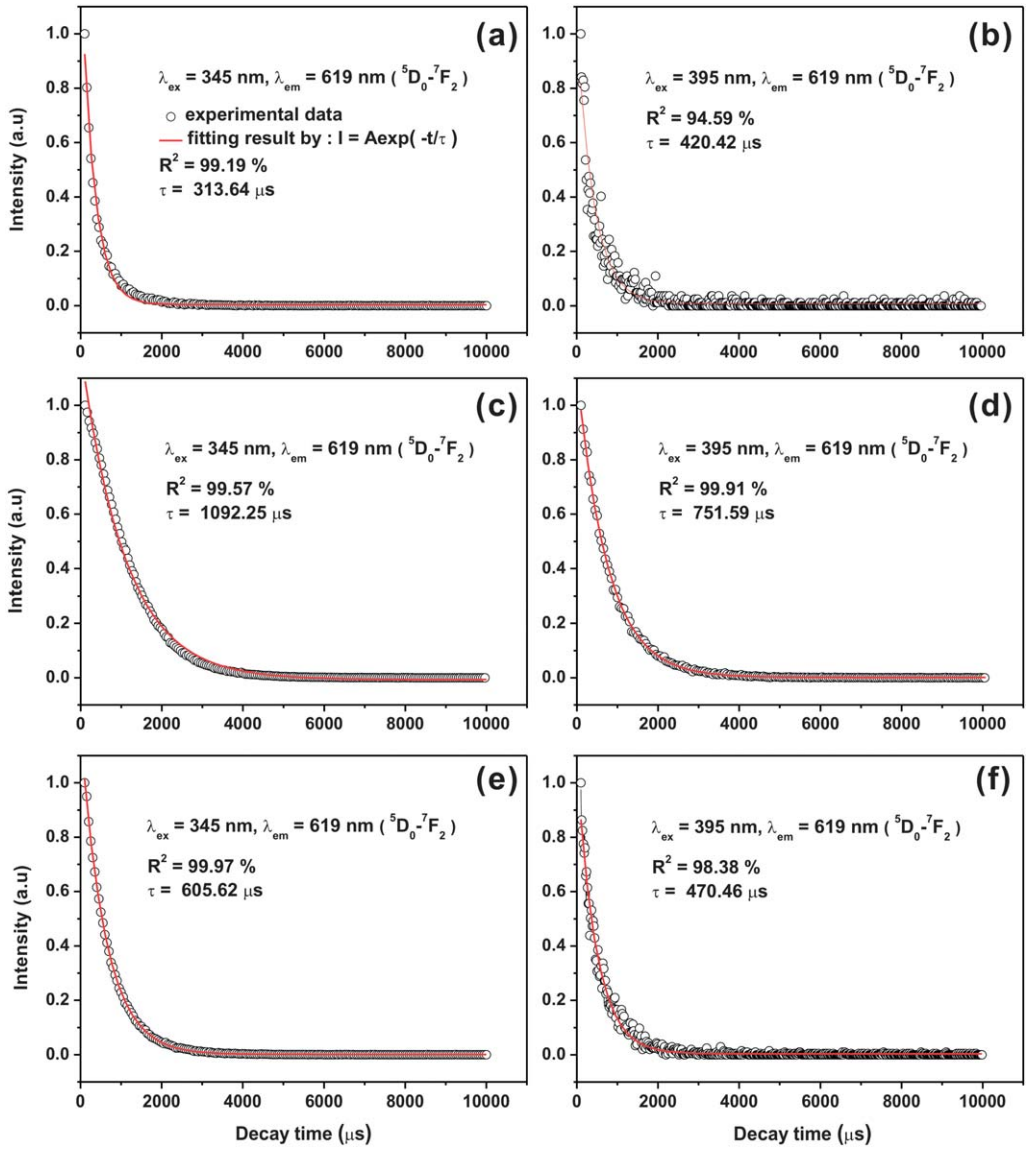


**Fig. 10** Photoluminescence decay curves for $Eu^{3+}$ emission ($^5D_0$–$^7F_2$) under 345 nm and 395 nm excitations for $YVO_4:Bi^{3+},Eu^{3+}$ nanocrystals. Samples were prepared by the hydrothermal method at (a,b) pH = 4, (c,d) pH = 7, (e,f) pH = 11.

under 345 and 395 nm excitations. The excitation peaks at 345 and 395 nm correspond to the excitation band of $Bi^{3+}$ and the $^7F_0$–$^5L_6$ sharp line excitation of the $Eu^{3+}$ f–f transition, respectively. The obtained decay curve can be well-fitted by the first-order exponential function, $I = A\exp(-t/\tau)$, where $I$ is the luminescence intensity at time $t$, $A$ is a constant, and $\tau$ is the decay lifetime for the exponential components. The measurement results of the luminescence lifetime of the as-synthesized samples at different pH values were reported with an accuracy ($R^2$) of 95–99%. For the 619 nm emission at a 345 nm excitation, the luminescence lifetimes are calculated to be 313.64, 1092.25 and 605.62 μs, which correspond to the samples prepared at pH = 4, 7 and 11, respectively. Moreover, the lifetime values are determined to be 420.42, 751.59 and 470.46 μs for the samples prepared at pH = 4, 7 and 11, at a 395 nm excitation, respectively. The values are in accordance with those given in the literature for the bulk (525 μs)[20] and nanocrystalline (740 μs)[35] materials. It can be observed that the sample prepared at pH = 7 exhibits a longer decay time than the others. We suggest that the increase in the lifetime is due to the decrease in the surface effects, as well as an improvement of the crystallinity. The luminescence of $Eu^{3+}$ on the nanocrystallite surface sites is easily quenched by combinations of solvent, or capping molecules. The polycrystalline product prepared at pH = 11 shows strong surface effects, leading to a decrease of the decay time value. The sample prepared at pH = 4 shows a much faster decay time of the $Eu^{3+}$ $^5D_0$–$^7F_2$ emission (619 nm) under the 345 nm excitation of $Bi^{3+}$. We assume that most of the $Bi^{3+}$ ions exhibit low reaction activities to produce the $YVO_4$:$Bi^{3+}$,$Eu^{3+}$ nanocrystals at pH = 4, and the concentration of $Bi^{3+}$ may involve the energy transfer rate from $Bi^{3+}$ to the $Eu^{3+}$ ion, correlated to the decay lifetime value.

### 3.4 Biomolecule conjugation

The surface-modified nanophosphors synthesized at pH = 7 can be well dispersed in DIW, and they show strong fluorescence properties. The surface amino groups provided from BPEI are activated by EDC, together with Sulfo-NHS, and can then covalently conjugate to the carboxyl groups of biomolecules. In our report, the obtained $YVO_4$:$Bi^{3+}$,$Eu^{3+}$ nanocrystals were conjugated with BSA in order to evaluate the binding ability related to the conjugated biomolecules. The successful conjugation of BSA with $YVO_4$:$Bi^{3+}$,$Eu^{3+}$ nanocrystals was proven by

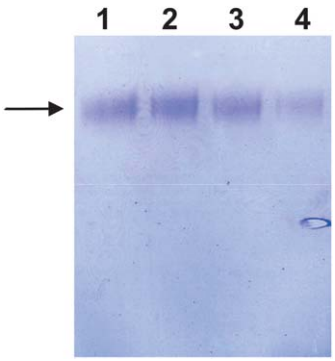


**Fig. 11** SDS-PAGE of the supernatant BSA after conjugation with 0 (lane 1), 0.1 (lane 2), 0.5 (lane 3), and 1.0 mg ml$^{-1}$ (lane 4) of $YVO_4$:$Bi^{3+}$,$Eu^{3+}$ nanocrystals.

**Table 2** The correlation between the $YVO_4$:$Bi^{3+}$,$Eu^{3+}$ NC concentration and the conjugated BSA concentration

| | NCs/mg ml$^{-1}$ | [BSA]/μg ml$^{-1}$ |
|---|---|---|
| 1 | 0 | 44.9 |
| 2 | 0.1 | 44.4 |
| 3 | 0.5 | 30.9 |
| 4 | 1.0 | 20.0 |

SDS-PAGE and a BCA protein assay (Fig. 11). Lane 1 is pure BSA before conjugation, and the un-conjugated BSA (supernatant) can be separated from the BSA-$YVO_4$:$Bi^{3+}$,$Eu^{3+}$ nanocrystal conjugates (pellet) by centrifugation treatment. It can be seen that the concentration of supernatant BSA decreases, while the $YVO_4$:$Bi^{3+}$,$Eu^{3+}$ nanocrystal concentration increases from 0.1 mg ml$^{-1}$ to 1.0 mg ml$^{-1}$. The quantity of conjugated BSA is determined by the difference in the UV absorbance values of the BCA solution before and after conjugation. This reveals that about 20 μg of BSA is associated per mg of $YVO_4$:$Bi^{3+}$,$Eu^{3+}$ nanocrystals (Table 2).

## 4. Conclusions

In this work, we have successfully synthesized $YVO_4$:$Bi^{3+}$,$Eu^{3+}$ nanocrystals with surface functionalization *via* a one-step BPEI-modified hydrothermal method. The water-based system provides a simple, solvent-free and safe green chemical synthesis route for nanomaterial preparation. The crystal structures, morphological evolution, photoluminescence properties and surface characterization were studied in detail. The crystal morphologies and particle sizes reveal diversities through a series of controlled experimental parameters, such as the reaction pH value and the concentration of capping agent. The obtained $YVO_4$:$Bi^{3+}$,$Eu^{3+}$ $YVO_4$:$Bi^{3+}$,$Eu^{3+}$ nanocrystals show a strong red luminescence (619 nm) under near-ultraviolet (n-UV) excitation. The surface amino groups contributed from the capping agent BPEI not only improve the dispersibility and water/buffer stability of the $YVO_4$:$Bi^{3+}$,$Eu^{3+}$ nanocrystals, but can also specifically conjugate with such biomolecules as folic acid, DNA or antibodies, for further applications in bioimaging, cell labeling and drug delivery. Moreover, the long luminescence lifetime and photoluminescence stability of the $YVO_4$:$Bi^{3+}$,$Eu^{3+}$ nanocrystals overcome the limitations of organic dyes. In conclusion, the $YVO_4$:$Bi^{3+}$,$Eu^{3+}$ nanocrystals with good water/buffer dispersibility, surface functionalization and long-lived red luminescence exhibit good potential for applications in bioimaging, DNA hybridization, fluorometric immunoassays and drug delivery.

## Acknowledgements

This research was supported by the National Science Council of Taiwan (R.O.C.) under Contract no. NSC98-2113-M-009-005-MY3. We thank Dr Yu-Kuo Wang for assistance in the helpful suggestions.

## Notes and references

1 L. Wang, R. Yan, Z. Huo, L. Wang, J. Zeng, J. Bao, X. Wang, Q. Peng and Y. Li, *Angew. Chem., Int. Ed.*, 2005, **44**, 6054.
2 N. C. Tansil and Z. Gao, *Nano Today*, 2006, **1**, 28.
3 S. Matthias, *Biosens. Bioelectron.*, 2005, **20**, 2454.

 

4 L. Wang and W. Tan, *Nano Lett.*, 2005, **6**, 84.
5 H. Guo, N. M. Idris and Y. Zhang, *Langmuir*, 2011, **27**, 2854.
6 W.-H. Chan, N.-H. Shiao and P.-Z. Lu, *Toxicol. Lett.*, 2006, **167**, 191.
7 C. Kirchner, T. Liedl, S. Kudera, T. Pellegrino, A. Muñoz Javier, H. E. Gaub, S. Stölzle, N. Fertig and W. J. Parak, *Nano Lett.*, 2005, **5**, 331.
8 J.-C. G. Bünzli, *Chem. Rev.*, 2010, **110**, 2729.
9 Z. Q. Li, Y. Zhang and S. Jiang, *Adv. Mater.*, 2008, **20**, 4765.
10 S. Setua, D. Menon, A. Asok, S. Nair and M. Koyakutty, *Biomaterials*, 2010, **31**, 714.
11 J. Chen, C. Guo, M. Wang, L. Huang, L. Wang, C. Mi, J. Li, X. Fang, C. Mao and S. Xu, *J. Mater. Chem.*, 2011, **21**, 2632.
12 D. K. Chatterjee, A. J. Rufaihah and Y. Zhang, *Biomaterials*, 2008, **29**, 937.
13 F. Vetrone, R. Naccache, A. Juarranz de la Fuente, F. Sanz-Rodriguez, A. Blazquez-Castro, E. M. Rodriguez, D. Jaque, J. G. Sole and J. A. Capobianco, *Nanoscale*, 2010, **2**, 495.
14 W. Xu, H. Song, D. Yan, H. Zhu, Y. Wang, S. Xu, X. Bai, B. Dong and Y. Liu, *J. Mater. Chem.*, 2011, **21**, 12331.
15 A. Huignard, T. Gacoin and J.-P. Boilot, *Chem. Mater.*, 2000, **12**, 1090.
16 R. A. Fields, M. Birnbaum and C. L. Fincher, *Appl. Phys. Lett.*, 1987, **51**, 1885.
17 M. Haase, K. Riwotzki, H. Meyssamy and A. Kornowski, *J. Alloys Compd.*, 2000, **303–304**, 191.
18 K. S. Sohn, J. M. Lee and N. Shin, *Adv. Mater.*, 2003, **15**, 2081.
19 A. Huignard, V. Buissette, A.-C. Franville, T. Gacoin and J.-P. Boilot, *J. Phys. Chem. B*, 2003, **107**, 6754.
20 A. K. Levine and F. C. Palilla, *Appl. Phys. Lett.*, 1964, **5**, 118.
21 R. C. Ropp, *J. Electrochem. Soc.*, 1968, **115**, 940.
22 G. Jia, K. Liu, Y. Zheng, Y. Song and H. You, *Cryst. Growth Des.*, 2009, **9**, 3702.
23 Y.-S. Chang, F.-M. Huang, Y.-Y. Tsai and L.-G. Teoh, *J. Lumin.*, 2009, **129**, 1181.
24 Z. Hou, P. Yang, C. Li, L. Wang, H. Lian, Z. Quan and J. Lin, *Chem. Mater.*, 2008, **20**, 6686.
25 M. N. Luwang, R. S. Ningthoujam, S. K. Srivastava and R. K. Vatsa, *J. Mater. Chem.*, 2011, **21**, 5326.
26 T. Taniguchi, T. Watanabe, K.-i. Katsumata, K. Okada and N. Matsushita, *J. Phys. Chem. C*, 2010, **114**, 3763.
27 Z. Xu, X. Kang, C. Li, Z. Hou, C. Zhang, D. Yang, G. Li and J. Lin, *Inorg. Chem.*, 2010, **49**, 6706.
28 G. Jia, Y. Song, M. Yang, Y. Huang, L. Zhang and H. You, *Opt. Mater.*, 2009, **31**, 1032.
29 K. Riwotzki and M. Haase, *J. Phys. Chem. B*, 1998, **102**, 10129.
30 B. C. Chakoumakos, M. M. Abraham and L. A. Boatner, *J. Solid State Chem.*, 1994, **109**, 197.
31 G. J. Koper, R. C. van Duijvenbode, D. D. P. W. Stam, U. Steuerle and M. Borkovec, *Macromolecules*, 2003, **36**, 2500.
32 S. Kobayashi, K. Hiroishi, M. Tokunoh and T. Saegusa, *Macromolecules*, 1987, **20**, 1496.
33 K.-J. Liu, *Macromolecules*, 1968, **1**, 390.
34 D. Chen, Y. Yu, P. Huang, H. Lin, Z. Shan, L. Zeng, A. Yang and Y. Wang, *Phys. Chem. Chem. Phys.*, 2010, **12**, 7775.
35 K. Riwotzki and M. Haase, *J. Phys. Chem. B*, 2001, **105**, 12709.